Mode Conversion Losses in Expansion Units for ITER ECH Transmission Lines

Citation: Schaub, S. C., M. A. Shapiro, R. J. Temkin, and G. R. Hanson. "Mode Conversion Losses in Expansion Units for ITER ECH Transmission Lines." J Infrared Milli Terahz Waves 37, no. 1 (August 16, 2015): 72–86.

As Published: http://dx.doi.org/10.1007/s10762-015-0190-4

Publisher: Springer US

Persistent URL: http://hdl.handle.net/1721.1/106984

Version: Author's final manuscript: final author's manuscript post peer review, without publisher's formatting or copy editing

J Infrared Milli Terahz Waves manuscript No.
(will be inserted by the editor)

Mode Conversion Losses in Expansion Units for ITER ECH Transmission Lines

S. C. Schaub · M. A. Shapiro · R. J. Temkin · G. R. Hanson

Received: date / Accepted: date

Abstract The ITER electron cyclotron heating transmission lines will consist of 63.5 mm diameter corrugated waveguides, each carrying 1 MW of 170 GHz microwaves. These transmission lines must include expansion units to accommodate expansion and contraction along the path from the gyrotron microwave sources to the tokamak. A numerical mode matching code has been developed to calculate power losses due to mode conversion of the operating mode, HE_{11}, to higher order modes as a result of the radial discontinuities in a sliding joint. Two expansion unit designs were evaluated, a simple gap expansion unit and a more complex tapered expansion unit. The gap expansion unit demonstrated loss that oscillated rapidly with expansion length, due to trapped modes within the unit. The tapered expansion unit has been shown to effectively suppress these trapped modes at the expense of increased fabrication complexity. In a gap expansion unit, for a waveguide step size of 2.5 mm, loss can be kept below 0.1% to a maximum expansion length of 17 mm. Expansion units without corrugation on interior walls were also evaluated. Expansion units that lack corrugations are found to increase mode trapping within the units, though not beyond useful application. The mode matching code developed in this paper was also used to estimate mode conversion loss in vacuum pumpouts for the ECH lines; the estimated loss was found to be negligibly small.

Keywords ITER, electron cyclotron heating, transmission line, gyrotron

S. C. Schaub · M. A. Shapiro · R. J. Temkin
Plasma Science & Fusion Center, Massachusetts Institute of Technology
167 Albany St., Bldg. NW16, Cambridge, MA 02139, USA
E-mail: shapiro@psfc.mit.edu

G. R. Hanson
US ITER Project
Oak Ridge National Laboratory
Oak Ridge, TN 37831, USA

1 Introduction

Electron cyclotron heating (ECH) and electron cyclotron current drive (ECCD) in ITER will be initially provided by twenty-four, 1 MW, 170 GHz gyrotrons [1–3]. The gyrotron systems will reside in a separate building from the tokamak. Transmission lines, consisting of 63.5 mm diameter corrugated waveguide, will carry power from the gyrotron systems to the ECH launchers mounted on the tokamak. The long transmission lines will require sliding joints. These will accommodate positional shifts between the tokamak building, assembly building, and the RF building, as well as thermal expansion and contraction.

ITER specifications have placed stringent requirements upon acceptable losses in the ECH transmission lines. The overall efficiency of the transmission lines, from the gyrotron matching optics units to the plasma facing diamond windows, with a transmission length of up to 150 m, must be at least 90%. The challenge to meet the ITER requirement on transmission losses is a topic of intensive present-day research [4–15].

In Section 2, a mode matching code is developed to calculate mode conversion between azimuthally symmetric modes of either corrugated or smooth-walled waveguide. In Sections 3-5, our mode matching code is benchmarked and used to evaluate mode conversion loss in transmission line expansion units of various designs. In Section 6, our mode matching code is used to estimate losses in a model pumpout for the ITER transmission lines. Section 7 presents a discussion and conclusions.

2 Mode Matching Code

2.1 Mode Matching Code Overview

Results are presented of a numerical mode matching code that we have developed to calculate mode conversion losses due to radial discontinuities in highly overmoded waveguides. The code was developed to analyze either smooth or corrugated waveguides. The performance of the code was benchmarked against diffractive loss in a waveguide gap, as calculated in [16], and, for the TE_{01} mode of smooth cylindrical waveguide, against the commercial software Ansys High Frequency Structural Simulator (HFSS). After validation, the code was used to evaluate two expansion unit designs, defined in Fig. 1. The gap expansion unit uses a simple radial step to a larger diameter. The tapered expansion unit includes a tapered transition to a larger diameter section, but retains an abrupt step back down to the original waveguide diameter. The abrupt step remains so that all parts may be suitably thick to survive heat load due to losses. It is assumed that there is no power lost due to the small space between the fixed and sliding surfaces. Ohmic loss is also not considered in this study. For calculations of loss in the HE_{11} mode, the expansion units shown in Fig. 1 have corrugated walls on all straight sections and tapers, except as noted in Section 5 of this paper.

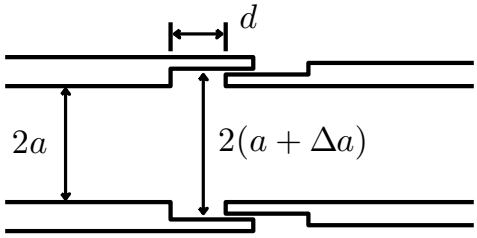

(a) Gap expansion unit

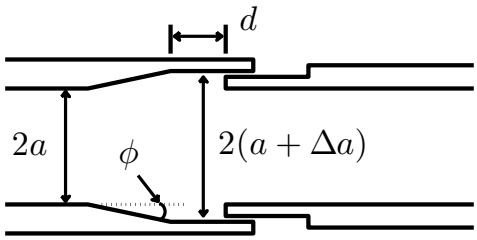

(b) Tapered expansion unit

Fig. 1: Geometry of the two waveguide expansion unit designs under consideration. Units were simulated with smooth walls using TE_{0n} modes, for benchmarking purposes, and corrugated walls using HE_{1n} modes for application.

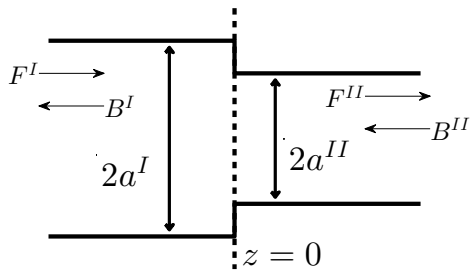

Fig. 2: Geometry for the derivation of scattering matrices. Forward and backward going waves are considered in the regions before and after the radial discontinuity at z = 0.

2.2 Derivation of Scattering Matrices for Mode Matching Code

Mode conversion due to a single radial discontinuity was calculated following the mode matching techniques and scattering matrix formulations outlined in [17,18]. Mode conversion was derived for a transition from larger to smaller radius, as shown in Fig. 2. Only symmetric modes were considered in this analysis, i.e. TE_{0n} and HE_{1n} modes in smooth and corrugated waveguide, respectively. Mode conversion for TE_{0n} and HE_{1n} modes were derived in parallel to allow benchmarking with HFSS. The approach used here is similar to that used to calculate the over-

all scattering matrices of complex cavities in [19] and modes excited in dielectric windows in [20].

The electric and magnetic fields of smooth and corrugated waveguides are given by Eqs. 1-10. The fields for TE_{0n} modes are given in Eqs. 1 - 5. The amplitude of the forward going wave in each region is given by F and the amplitude of the backward going waves is given by B.

$$\langle E_\varphi \rangle^I_{\mathrm{TE}_{0n}} = \sum_n A^I_n J_1\left(\frac{\nu'_n r}{a^I}\right)\left(F^I_n e^{-ik^I_{zn}z} + B^I_n e^{ik^I_{zn}z}\right) \tag{1}$$

$$\langle H_r \rangle^I_{\mathrm{TE}_{0n}} = \sum_n \frac{-A^I_n k^I_{zn}}{\mu_0 \omega} J_1\left(\frac{\nu'_n r}{a^I}\right)\left(F^I_n e^{-ik^I_{zn}z} - B^I_n e^{ik^I_{zn}z}\right) \tag{2}$$

$$\langle E_\varphi \rangle^{II}_{\mathrm{TE}_{0m}} = \sum_m A^{II}_m J_1\left(\frac{\nu'_m r}{a^{II}}\right)\left(F^{II}_m e^{-ik^{II}_{zm}z} + B^{II}_m e^{ik^{II}_{zm}z}\right) \tag{3}$$

$$\langle H_r \rangle^{II}_{\mathrm{TE}_{0m}} = \sum_m \frac{-A^{II}_m k^{II}_{zm}}{\mu_0 \omega} J_1\left(\frac{\nu'_m r}{a^{II}}\right)\left(F^{II}_m e^{-ik^{II}_{zm}z} - B^{II}_m e^{ik^{II}_{zm}z}\right) \tag{4}$$

$$k^I_{zn} = \sqrt{\frac{\omega^2}{c^2} - \left(\frac{\nu'_n}{a^I}\right)^2}; \quad k^{II}_{zm} = \sqrt{\frac{\omega^2}{c^2} - \left(\frac{\nu'_m}{a^{II}}\right)^2} \tag{5}$$

The coordinate z is along the axis of the waveguide and r is radial distance away from the axis. The value ν'_n is the nth zero of J_1, a first order Bessel function of the first kind. The wavenumber parallel to z is k_z, μ_0 is the permeability of free space, c is the speed of light in vacuum, and ω is the angular frequency of the input microwave. Subscript m or n indicates the number of the waveguide mode, ordered by cutoff frequency. Superscript I or II indicates that the value is evaluated before or after the radial discontinuity, respectively. In all calculations presented here, $\omega = 2\pi \times 170$ GHz. The electric and magnetic fields of the HE_{1n} modes with linear polarization along the y-axis are given in Eqs. 6 - 10. These are approximations to the dominant components of the HE_{1n} modes for corrugations of quarter wavelength depth as found in [21].

$$\langle E_y \rangle^I_{\mathrm{HE}_{1n}} = \sum_n A^I_n J_0\left(\frac{\nu_n r}{a^I}\right)\left(F^I_n e^{-ik^I_{zn}z} + B^I_n e^{ik^I_{zn}z}\right) \tag{6}$$

$$\langle H_x \rangle^I_{\mathrm{HE}_{1n}} = \sum_n \frac{-A^I_n k^I_{zn}}{\mu_0 \omega} J_0\left(\frac{\nu_n r}{a^I}\right)\left(F^I_n e^{-ik^I_{zn}z} - B^I_n e^{ik^I_{zn}z}\right) \tag{7}$$

$$\langle E_y \rangle^{II}_{\mathrm{HE}_{1m}} = \sum_m A^{II}_m J_0\left(\frac{\nu_m r}{a^{II}}\right)\left(F^{II}_m e^{-ik^{II}_{zm}z} + B^{II}_m e^{ik^{II}_{zm}z}\right) \tag{8}$$

$$\langle H_x \rangle^{II}_{\mathrm{HE}_{1m}} = \sum_m \frac{-A^{II}_m k^{II}_{zm}}{\mu_0 \omega} J_0\left(\frac{\nu_m r}{a^{II}}\right)\left(F^{II}_m e^{-ik^{II}_{zm}z} - B^{II}_m e^{ik^{II}_{zm}z}\right) \tag{9}$$

$$k^I_{zn} = \sqrt{\frac{\omega^2}{c^2} - \left(\frac{\nu_n}{a^I}\right)^2}; \quad k^{II}_{zm} = \sqrt{\frac{\omega^2}{c^2} - \left(\frac{\nu_m}{a^{II}}\right)^2} \tag{10}$$

Here ν_n is the nth zero of J_0, a zeroth order Bessel function of the first kind. The amplitudes, A^I_n, were found by setting the amplitude of the forward wave to

$F_n^I = 1$ and the amplitude of the backward wave to $B_m^{II} = 0$. At these parameters, the power in the mode is defined as equal to one watt. This yields for A_n^I:

$$\text{TE}_{0n} \text{ modes: } A_n^I = \sqrt{\frac{2\mu_0\omega}{\pi k_{zn}^I}} \frac{1}{a^I \left|J_0(\nu_n')\right|} \tag{11}$$

$$\text{HE}_{1n} \text{ modes: } A_n^I = \sqrt{\frac{2\mu_0\omega}{\pi k_{zn}^I}} \frac{1}{a^I \left|J_1(\nu_n)\right|} \tag{12}$$

Using this normalization, the electric and magnetic fields of the modes of region I were projected onto those of region II at the $z = 0$ discontinuity. The procedure is outlined below for projection of the electric fields of the HE_{1n} modes.

$$\langle E_y^I \rangle \Big|_{z=0} = \langle E_y^{II} \rangle \Big|_{z=0} \tag{13}$$

$$\sum_n \left\{ A_n^I J_0\left(\frac{\nu_n r}{a^I}\right) \left(F_n^I + B_n^I\right) \right\} = \sum_m \left\{ A_m^{II} J_0\left(\frac{\nu_m r}{a^{II}}\right) \left(F_m^{II} + B_m^{II}\right) \right\} \tag{14}$$

Both sides of Eq. 14 were multiplied by r and a Bessel function representing the electric field in the larger cross section, $J_0\left(\frac{\nu_l r}{a^I}\right)$. Integrating the resulting expression, Eq. 15, over the waveguide cross section allowed use of the orthogonality relationship for Bessel functions, Eq. 16, to pick out the projection of a single mode of region I onto all the modes of region II.

$$\begin{aligned} &\sum_n \left\{ A_n^I \left(F_n^I + B_n^I\right) \int_0^{a^I} r J_0\left(\frac{\nu_n r}{a^I}\right) J_0\left(\frac{\nu_l r}{a^I}\right) dr \right\} \\ &\quad = \sum_m \left\{ A_m^{II} \left(F_m^{II} + B_m^{II}\right) \left(\int_0^{a^{II}} r J_0\left(\frac{\nu_m r}{a^{II}}\right) J_0\left(\frac{\nu_l r}{a^I}\right) dr + \int_{a^{II}}^{a^I} 0 dr \right) \right\} \end{aligned} \tag{15}$$

$$\int_0^1 z J_\alpha\left(\nu_n z\right) J_\alpha\left(\nu_l z\right) dz = \frac{\delta_{nl}}{2} \left(J_{\alpha+1}\left(\nu_n\right)\right)^2 \tag{16}$$

$$\begin{aligned} &\frac{1}{2} A_n^I \left(a^I\right)^2 J_1^2\left(\nu_n\right) \left(F_n^I + B_n^I\right) \\ &\qquad = \sum_m \left\{ A_m^{II} \left(F_m^{II} + B_m^{II}\right) \left(\int_0^{a^{II}} r J_0\left(\frac{\nu_m r}{a^{II}}\right) J_0\left(\frac{\nu_n r}{a^I}\right) dr \right) \right\} \end{aligned} \tag{17}$$

The transmission matrices, L_E and L_H are defined in Eqs. 18 and 19. These can be read off from Eq. 17. It can be shown by using the above procedure to match the magnetic fields at the discontinuity that $L_E = L_H^T$. Superscript T stands for the transpose of the matrix.

$$\left(F_n^I + B_n^I\right) = \sum_m \left(L_E\right)_{nm} \left(F_m^{II} + B_m^{II}\right) \tag{18}$$

$$\sum_n \left(L_H\right)_{nm} \left(F_n^I - B_n^I\right) = \left(F_m^{II} - B_m^{II}\right) \tag{19}$$

By observation of close parallels between the equations describing the fields of the TE_{0n} and HE_{1n} modes, it can be concluded that equations derived for HE_{1n} modes can be simply transformed to those for the TE_{0n} modes, using the substitutions in Eq. 20. The final form for the transmission matrices is given in Eqs. 21 and 22, for the TE_{0n} and HE_{1n} modes, respectively. Scattering matrices are calculated from transmission matrices using Eq. 23.

$$J_0(z) \rightarrow J_1(z) \tag{20a}$$

$$\nu_n \rightarrow \nu'_n \tag{20b}$$

$$J_1(\nu_n) \rightarrow J_2(\nu'_n) = -J_0(\nu'_n) \tag{20c}$$

TE_{0n} modes:

$$(L_E)_{nm} = \left(\frac{k^I_{zn}}{k^{II}_{zm}}\right) \frac{a^I \left|J_0\left(\nu'_n\right)\right|}{a^{II} \left|J_0\left(\nu'_m\right)\right|} \frac{2}{\left(a^I\right)^2 J_0^2\left(\nu'_n\right)} \int_0^{a^{II}} r J_1\left(\frac{\nu'_n r}{a^I}\right) J_1\left(\frac{\nu'_m r}{a^{II}}\right) dr = (L_H)_{mn} \tag{21}$$

HE_{1n} modes:

$$(L_E)_{nm} = \left(\frac{k^I_{zn}}{k^{II}_{zm}}\right) \frac{a^I \left|J_1\left(\nu_n\right)\right|}{a^{II} \left|J_1\left(\nu_m\right)\right|} \frac{2}{\left(a^I\right)^2 J_1^2\left(\nu_n\right)} \int_0^{a^{II}} r J_0\left(\frac{\nu_n r}{a^I}\right) J_0\left(\frac{\nu_m r}{a^{II}}\right) dr = (L_H)_{mn} \tag{22}$$

$$S_{11} = [L_E L_H + I]^{-1}[L_E L_H - I] \tag{23a}$$

$$S_{12} = 2[L_E L_H + I]^{-1} L_E \tag{23b}$$

$$S_{21} = L_H\{I - S_{11}\} \tag{23c}$$

$$S_{22} = I - L_H S_{12} \tag{23d}$$

The case where $a^I < a^{II}$ is handled with a simple transformation: $S_{11} \leftrightarrow S_{22}$ and $S_{12} \leftrightarrow S_{21}$. Waves are propagated through straight waveguide with the scattering matrices given in Eq. 24.

$$S_{11} = S_{22} = 0 \tag{24a}$$

$$S_{12} = S_{21} = D \tag{24b}$$

D is an $N \times N$ diagonal matrix, with elements $D_{nm} = exp\left(-ik_{zn}L\right)\delta_{nm}$. N is the total number of modes used in the calculation. L is the length of the straight section of waveguide. Consecutive scattering matrices are cascaded via the formalism shown in Eq. 25. In this manner, an overall scattering matrix is calculated for the expansion unit under consideration.

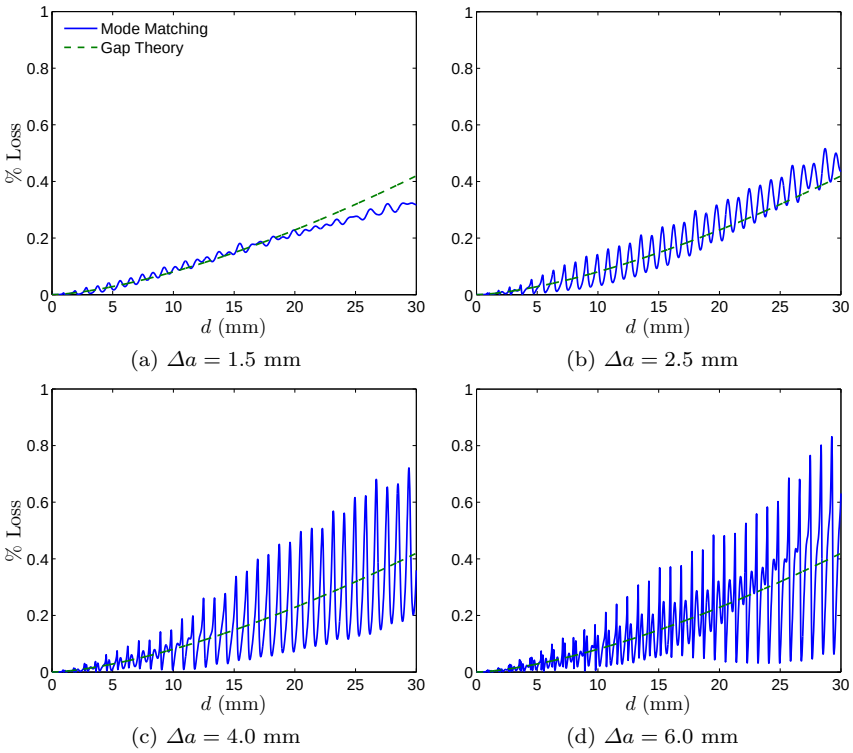

(a) $\Delta a = 1.5$ mm (b) $\Delta a = 2.5$ mm

(c) $\Delta a = 4.0$ mm (d) $\Delta a = 6.0$ mm

Fig. 3: Comparison of mode conversion loss of TE_{01} mode in the smooth waveguide gap expansion unit, as predicted by our mode matching code, and gap diffraction theory, Eq. 26. Plots a - d are for different values of Δa. The waveguide radius is $a = 31.75$ mm, and the frequency is 170.0 GHz.

$$S_{11} = S_{11}^{(1)} + S_{12}^{(1)} S_{11}^{(2)} W S_{12}^{(1)} \tag{25a}$$

$$S_{12} = S_{12}^{(1)} (I + S_{11}^{(2)} W S_{22}^{(1)}) S_{12}^{(2)} \tag{25b}$$

$$S_{21} = S_{21}^{(2)} W S_{21}^{(1)} \tag{25c}$$

$$S_{22} = S_{22}^{(2)} + S_{21}^{(2)} W S_{22}^{(1)} S_{12}^{(2)} \tag{25d}$$

$$W = [I - S_{22}^{(1)} S_{11}^{(2)}]^{-1} \tag{25e}$$

3 Mode Matching Results and Benchmarking for the TE_{01} Mode of Smooth Waveguide

Multiple methods were used to benchmark the performance of our mode matching code. As a first approximation, the losses were calculated using gap diffraction theory. This model radiates power in the desired mode from the exit of one waveguide

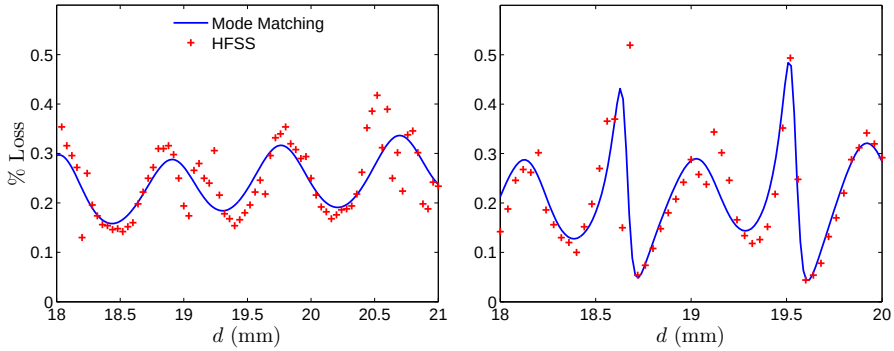

(a) $\Delta a = 2.5$ mm (b) $\Delta a = 6.0$ mm

Fig. 4: A zoomed in comparison of TE_{01} loss in the smooth waveguide gap expansion unit as predicted by our mode matching code and HFSS. The oscillations predicted by our code have a period of 0.89 mm, approximately $\lambda/2$.

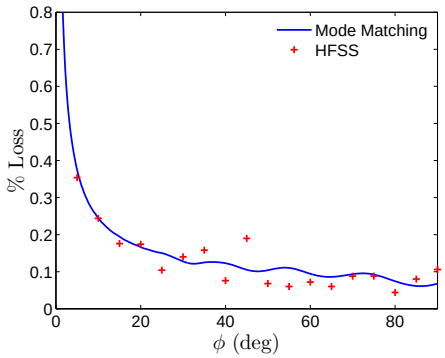

Fig. 5: Comparison of mode conversion loss of TE_{01} mode in the smooth waveguide tapered expansion unit versus taper angle as predicted by our mode matching code and HFSS. The model in this comparison uses a step size of $\Delta a = 2.5$ mm and an expansion length of $d = 10$ mm.

to the entrance of a second waveguide using diffraction theory. The power entering the second waveguide is projected onto the TE_{01} or HE_{11} modes for smooth or corrugated waveguide, respectively. Power that does not project onto the desired mode of the second waveguide is considered lost. This simple model will be found to be inaccurate for small values of step size, Δa, and at long gap lengths, d. This model also cannot account for trapped modes or reflections. However, this calculation is particularly useful because of its approximate validity for both TE_{01} and HE_{11} modes. The diffractive losses for radiation of wavelength λ across a gap of length d, between waveguides of radius a can be expressed analytically [16]. The losses of TE_{01} power radiating between smooth walled waveguides is given by Eq. 26. The losses of HE_{11} power radiating between corrugated waveguides is given by Eq. 27.

$$\mathrm{TE}_{01}\ fractional\ loss = 0.99\left(\frac{d\lambda}{2a^2}\right)^{3/2} \tag{26}$$

$$\mathrm{HE}_{11}\ fractional\ loss = 0.39\left(\frac{d\lambda}{2a^2}\right)^{3/2} \tag{27}$$

In addition, the code for TE_{0n} modes in a smooth, circular waveguide is benchmarked against the commercially available HFSS software. The HFSS code was used only to model the smooth-walled version of both the gap and tapered expansion units, because the fine mesh required to model corrugated walls would require computing power beyond our means. Simulations performed with HFSS are limited to the first 25 symmetric modes of the structure, ordered by cutoff frequency. Because of the highly overmoded nature of the ITER transmission lines, not all of the propagating TE_{0n} modes of the waveguides can be taken into account. However, HFSS does well model the complex behavior that arises due to trapped modes and reflections in the expansion units, allowing us to benchmark this aspect of our code.

In all results presented in this paper, calculations made with our mode matching code account for the first 100 symmetric modes of the waveguides. This includes all propagating modes and a sufficient number of evanescent modes to achieve convergence of our results for all the geometries under consideration. Fig. 3 shows the results of our code for the TE_{01} mode in a smooth-walled gap expansion unit versus the predictions of gap diffraction theory, Eq. 26. As expected, our results diverge from gap diffraction theory at small values of Δa and large expansion length. In addition, our results show rapid oscillation in loss versus expansion length. The oscillations have a period of 0.89 mm, approximately $\lambda/2$, as expected for trapped modes. To verify the reality of this behavior, Fig. 4 shows a detailed comparison of the results of HFSS and our code. It can be seen that HFSS reproduces the rapid oscillations seen in our own calculations. This benchmarking is a good confirmation of the accuracy of our mode matching code.

To apply our mode matching code to the tapered expansion unit, the taper was modeled as a series of radial steps. The number of steps was increased until the results of the calculations converged. 100 such steps were used in all results presented in this paper. Fig. 5 compares the results of HFSS and our code for the TE_{01} mode in a tapered expansion unit in smooth waveguide. Shown in this figure is a model with a step size of $\Delta a = 2.5$ mm and an expansion length of $d = 10$ mm. Our code and HFSS are shown to be in good agreement as the taper angle, ϕ, is swept from 5° to 90°.

4 Results for the HE_{11} Mode of Corrugated Waveguide in Fully Corrugated Expansion Units

The results of our calculations for loss of the HE_{11} mode in a corrugated gap expansion unit are shown in Fig. 6. Gap diffraction theory, Eq. 27, well predicts a moving average of our results for large values of Δa, as well as at small expansion length for small values of Δa. Rapid oscillations with expansion length increase in amplitude dramatically as the value of Δa is increased.

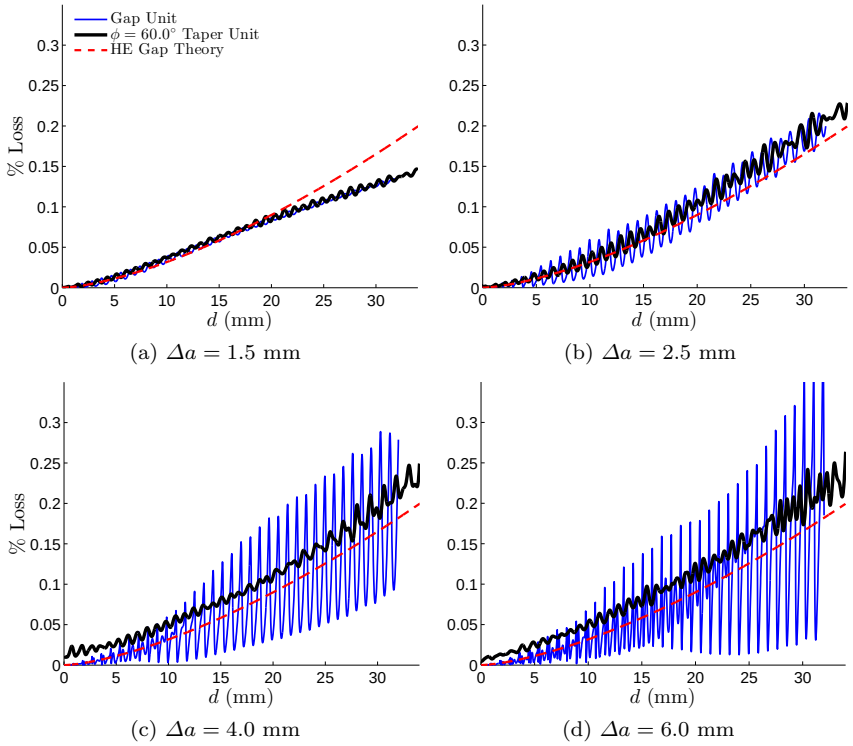

(a) $\Delta a = 1.5$ mm (b) $\Delta a = 2.5$ mm

(c) $\Delta a = 4.0$ mm (d) $\Delta a = 6.0$ mm

Fig. 6: Mode conversion loss of HE_{11} mode in the fully corrugated gap expansion unit, Fig. 1a, and tapered expansion unit, Fig. 1b, as predicted by our mode matching code. The predictions of gap diffraction theory, Eq. 27, are included for comparison. Plots a - d are for different values of Δa. The waveguide radius is $a = 31.75$ mm, and the frequency is 170.0 GHz.

Fig. 6 also includes the results for a tapered expansion unit with a taper angle of $\phi = 60°$. For these calculations, all inner surfaces are assumed to be corrugated, including the taper. The rapid oscillations in loss, resulting from trapped modes, are partially suppressed by the addition of a taper. This is most evident at expansion units with large step size, $\Delta a \geq 4$ mm. Fig. 7 shows results for a tapered expansion unit with a fixed step size of $\Delta a = 2.5$ mm as both taper angle, ϕ, and expansion length, d, are varied. It is shown that the amplitude of trapped modes decreases as taper angle decreases away from 90°. At very shallow taper angles, this advantage is mitigated by the additional losses in the taper, which leads to nonzero mode conversion even at zero expansion length. The example angle of $\phi = 60°$ shown in Fig. 6 was chosen as a reasonable balance point between mode suppression and additional loss.

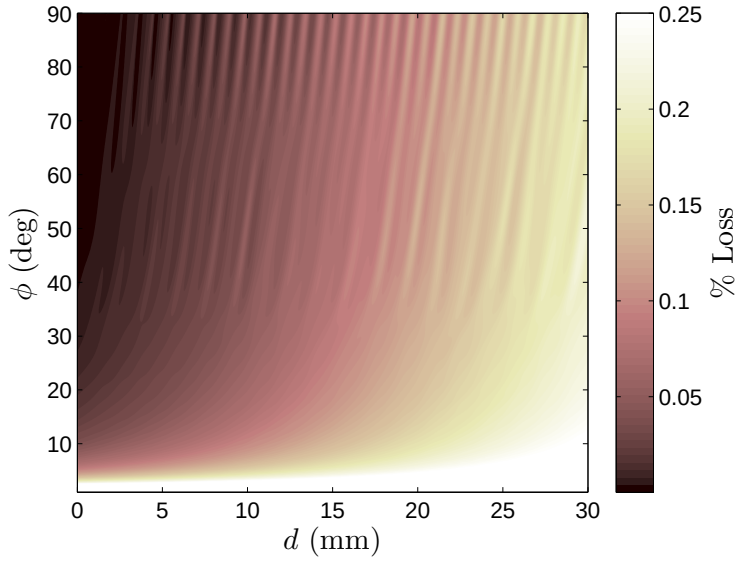

Fig. 7: Percent loss of HE_{11} mode in the corrugated tapered expansion unit as a function of the taper angle, ϕ, and expansion length, d, as predicted by our mode matching code. The step size used in this model is $\Delta a = 2.5$ mm. The waveguide radius is $a = 31.75$ mm, and the frequency is 170.0 GHz.

5 Gap Expansion Units with Smooth Wall Sections

The approximate accuracy of gap diffraction theory suggests that it may not be necessary to corrugate all the surfaces of the expansion units. In this section, expansion units in which certain walls are not corrugated are evaluated. Both designs shown in Fig. 1 are considered. In the designs shown in Fig. 1, the sections of waveguide with radius $r = a+\Delta a$ have smooth walls. All the surfaces with radius $r = a$ have corrugated walls. For the tapered design shown in Fig. 1b, the taper has a smooth wall. To evaluate the transmission of these units, the commercially available Cascade software, [22], was used to calculate scattering matrices for the smooth section of each expansion unit. The first 100 TE_{1n} and TM_{1n} modes were used, ordered by cutoff frequency. The HE_{11} mode of corrugated waveguide was projected onto the TE_{1n} and TM_{1n} modes of smooth circular waveguide, using scattering matrices from [23]. Eq. 28 projects the HE_{11} mode onto TE_{1n} modes. Eq. 29 projects the HE_{11} mode onto TM_{1n} modes. The constants $\nu_{m,n}$ and $\nu'_{m,n}$ correspond to the nth zero of J_m and J'_m, respectively.

$$S_{21} = \frac{\sqrt{2}\nu_{0,1}}{(\nu_{0,1})^2 - (\nu'_{1,n})^2} \frac{1}{\sqrt{(\nu'_{1,n})^2 - 1}} \frac{J_0(\nu'_{1,n})}{|J_0(\nu'_{1,n})|}, \; HE_{11} \rightarrow TE_{1n} \tag{28}$$

$$S_{21} = \frac{\sqrt{2}\nu_{0,1}}{(\nu_{0,1})^2 - (\nu_{1,n})^2} \frac{J_0(\nu_{1,n})}{|J_0(\nu_{1,n})|}, \; HE_{11} \rightarrow TM_{1n} \tag{29}$$

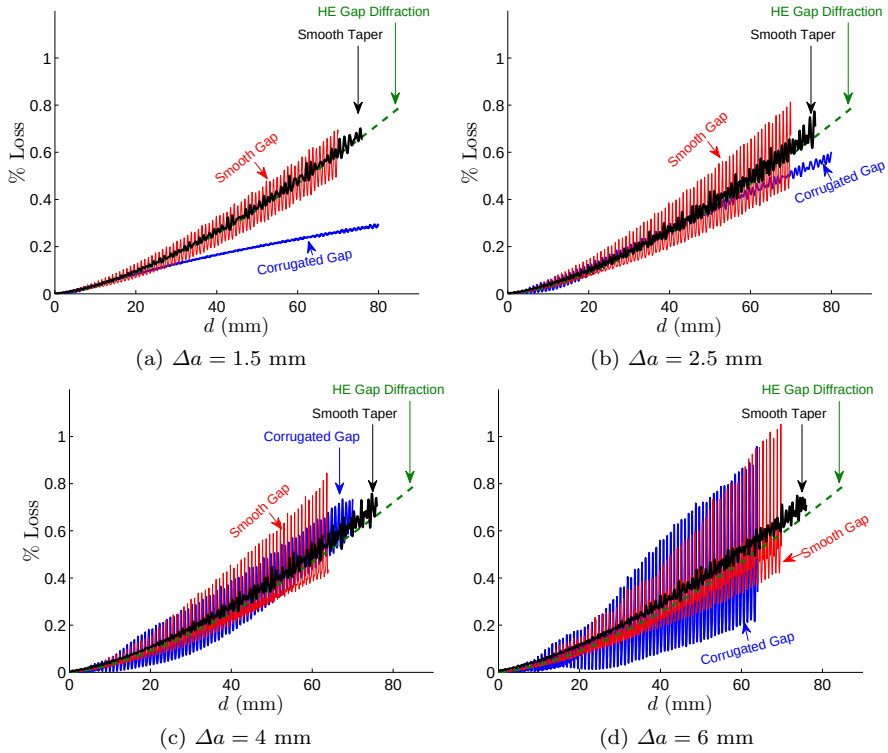

(a) $\Delta a = 1.5$ mm (b) $\Delta a = 2.5$ mm

(c) $\Delta a = 4$ mm (d) $\Delta a = 6$ mm

Fig. 8: Loss of the HE_{11} mode in expansion units with and without corrugation on the interior walls. The *corrugated gap* line represents the gap expansion unit of Fig. 1a with all walls corrugated. The *smooth gap* line represents the same unit with a smooth wall on the section of waveguide with radius $r = a + \Delta a$. The *smooth taper* line represents the tapered expansion unit of Fig. 1b with a smooth wall on both the taper and the section of straight waveguide with radius $r = a + \Delta a$. The taper angle on these units is $\phi = 60°$. The predictions of gap diffraction theory, Eq. 27, included as a reference, are represented by the *HE gap diffraction* line. Plots a - d correspond to different step sizes, Δa.

The results of these calculations are displayed in Fig. 8. The removal of corrugations on the interior surfaces of the expansion units has several effects. The moving average of the loss remains in agreement with the predictions of gap diffraction theory, Eq. 27, to much longer expansion lengths. In contrast, loss in the fully corrugated expansion units tends to be lower at long expansion lengths. Additionally, the amplitude of the oscillations in loss versus length due to trapped modes behaves differently as parameters are varied. In units with smooth walls, the amplitude of oscillations has a significantly weaker dependence on both step size, Δa, and expansion length, d. For the suppression of trapped modes, this is unfavorable at small step sizes and very short distances, but may be advantageous for the design of units with a large step size of $\Delta a \gtrsim 6$ mm.

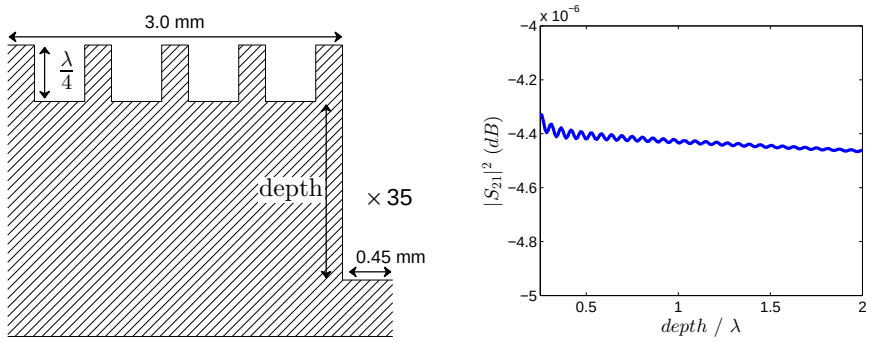

(a) Approximation of Pumpout (b) Transmission of HE_{11} mode

Fig. 9: Approximation of mode conversion loss in a waveguide pumpout. a) One period of the model waveguide wall used to simulate the pumpout slots. b) Transmission of HE_{11} mode through a pumpout containing 35 periods.

The plots of Fig. 8 show loss to longer expansion lengths than the previous plots. It is an ideal situation to limit expansion lengths to no more than $d = 30$ mm, where mode conversion losses per expansion unit can be kept very low. However, long runs of transmission line in the RF building, as well as transient environmental conditions may necessitate expansion gaps of 50 mm or more. As can be seen in Fig. 8, fully corrugated units have a significant advantage at long expansion lengths only if the step size, Δa, is less than about 4 mm.

The addition of a taper to one side of the expansion unit is an effective method of suppressing trapped modes at long expansion lengths regardless of step size, at least up to $\Delta a = 6$ mm. The units evaluated in Fig. 8 have a taper angle of $\phi = 60°$. For clarity in the plots of Fig. 8, the results for the fully corrugated tapered unit are omitted. The behavior of these units at long expansion lengths continues to follow the pattern shown in Fig. 6. The moving average continues to track close to that of the fully corrugated gap expansion unit, though with smaller amplitude oscillations due to suppression of trapped modes.

6 ITER Waveguide Pumpouts

The mode matching code developed in this paper was used to estimate mode conversion losses in vacuum pumpouts for the ITER ECH waveguide. Because the code is limited to axially symmetric waveguides, a simplified model of a pumpout was analyzed. Shown in Fig. 9a, a corrugated waveguide in which a slot is cut into every fifth corrugation was analyzed. For a pumpout, the slot must go through the waveguide wall. To approximate mode conversion losses, the depth of the slot was increased until the asymptotic behavior of the system was determined.

The pumpout model analyzed included 35 slots in a total of 12.075 cm of waveguide. 350 modes were accounted for in the calculation to achieve convergence of the results shown in Fig. 9b. Mode conversion loss due to the narrow slots was calculated to be very small. Transmission loss of the HE_{11} mode is approximately -4.5×10^{-6} dB for the pumpout. This is less than the expected ohmic loss in 12

cm of ITER ECH waveguide, 1.9×10^{-5} dB, estimated using expressions found in [24,25].

7 Discussion and Conclusions

It has been shown that, for sufficiently small expansion length and radial step size, mode conversion losses in sliding waveguide joints of overmoded, corrugated waveguide can be kept acceptably low for use in the ECH system of ITER. Reflections and trapped modes in the expansion units lead to losses that oscillate rapidly with expansion length, with a period on the order of half the guide wavelength. This oscillation is too rapid to allow for optimization of the expansion units, but rather will lead to a range of predicted loss in each unit. It is seen that the addition of a tapered section of waveguide can be used to suppress these trapped modes. The decision to use a taper will depend upon the final design goals for the system. At the example step size of $\Delta a = 2.5$ mm, mode conversion loss can be kept below 0.1% to a maximum expansion length of $d = 17$ mm in the gap expansion unit. At this step size, conditions causing expansion gaps up to $d = 50$ mm will lead to losses of approximately 0.5%.

Losses have been calculated for expansion units that include a tapered section of waveguide. The tapered, corrugated waveguide was used at the non-moving side of the expansion unit. The taper allows for suppression of trapped modes in the unit. A second taper at the moving side of the expansion unit may result in more complete suppression of the trapped modes. This would, however, introduce additional complexity in the fabrication of the expansion units and necessitate thin, fragile parts.

Comparison of the results of the mode matching code with gap diffraction theory, Eq. 27, yields additional insight. Though the gap diffraction theory does not capture the effect of reflections, for sufficiently large values of Δa or short expansion lengths, the theory well approximates the moving average of our mode matching results. It is shown in Fig. 8 that, where our mode matching results and predictions of gap diffraction theory are in approximate agreement, corrugations on the walls of the larger radius waveguide do not affect the moving average of loss in the expansion unit. The trapping of modes and the resulting oscillations in loss versus expansion length, however, are affected by the presence of corrugations.

It is important to note that our calculations make an assumption of perfect axial alignment of the waveguides and expansion units. In application, slight tilts between waveguides can lead to higher order mode excitation, calculated in [21]. Specifically, a tilt as small as 0.045° can lead to 0.1% power losses as a result of conversion to the LP_{11} mode of the corrugated waveguide. Such alignment losses must be taken into account in the final design of the ITER waveguide expansion units.

Acknowledgments

This research was supported by the U.S. Department of Energy, Office of Fusion Energy Sciences, and by the U.S. ITER Project managed by Battelle / Oak Ridge National Laboratory.

References

1. F. Gandini, T. S. Bigelow, B. Becket, J. B. Caughman, D. Cox, C. Darbos, T. Gassmann, M. A. Henderson, O. Jean, K. Kajiwara, N. Kobayashi, C. Nazare, Y. Oda, T. Omori, D. Purohit, D. A. Rasmussen, D. M. S. Ronden, G. Saibene, K. Sakamoto, M. A. Shapiro, K. Takahashi, R. J. Temkin, *Fusion Sci. Technol.* **59**(4), 709 (2011).
2. T. Omori, M. A. Henderson, F. Albajar, S. Alberti, U. Baruah, T. S. Bigelow, B. Beckett, R. Bertizzolo, T. Bonicelli, A. Bruschi, J. B. Caughman, R. Chavan, S. Cirant, A. Collazos, D. Cox, C. Darbos, M.R. de Baar, G. Denisov, D. Farina, F. Gandini, T. Gassmann, T. P. Goodman, R. Heidinger, J. P. Hogge, S. Illy, O. Jean, J. Jin, K. Kajiwara, W. Kasparek, A. Kasugai, S. Kern, N. Kobayashi, H. Kumric, J. D. Landis, A. Moro, C. Nazare, Y. Oda, I. Pagonakis, B. Piosczyk, P. Platania, B. Plaum, E. Poli, L. Porte, D. Purohit, G. Ramponi, S. L. Rao, D. A. Rasmussen, D. M. S. Ronden, T. Rzesnicki, G. Saibene, K. Sakamoto, F. Sanchez, T. Scherer, M. A. Shapiro, C. Sozzi, P. Spaeh, D. Strauss, O. Sauter, K. Takahashi, R. J. Temkin, M. Thumm, M. Q. Tran, V. S. Udintsev, H. Zohm, *Fusion Eng. Des.*, **86**(6-8), 951 (2011).
3. Y. Oda, K. Kajiwara, K. Takahashi, A. Kasugai, M. A. Shapiro, R. J. Temkin, K. Sakamoto, *J. Infrared Millimeter Terahertz Waves* **31**(8), 949 (2010).
4. T. Shimozuma, H. Idei, M. A. Shapiro, R. J. Temkin, S. Kubo, H. Igami, Y. Yoshimura, H. Takahashi, S. Ito, S. Kobayashi, Y. Mizuno, Y. Takita, T. Mutoh, *Plasma Fusion Res.* **5**, S1029 (2010).
5. J. Lohr, Y. A. Gorelov, K. Kajiwara, D. Ponce, R. W. Callis, J. L. Doane, R. L. Ellis, H. J. Grunloh, C. P. Moeller, J. Peavey, R. Prater, J. F. Tooker, *Fusion Sci. Technol.* **48**(2), 1226 (2005).
6. R. A. Olstad, J. L. Doane, C. P. Moeller, *Fusion Eng. Des.*, **74**(1-4), 331 (2005).
7. J. L. Doane, R. A. Olstad, *Fusion Sci. Technol.*, **53**(1), 39 (2008).
8. J. L. Doane, *Fusion Sci. Technol.*, **53**(1), 159 (2008).
9. K. Kajiwara, K. Takahashi, N. Kobayashi, A. Kasugai, T. Kobayashi, K. Sakamoto, *Proc. Joint 32nd Int. Conf. Infrared and Millimeter Waves and the 15th Int. Conf. Terahertz Electronics (IRMMW-THz)*, Cardiff, United Kingdom, September 2–7, 2007, p. 793 (2008).
10. S. T. Han, E. N. Comfoltey, M. A. Shapiro, J. R. Sirigiri, D. S. Tax, R. J. Temkin, P. P. Woskov, D. A. Rasmussen, *Int. J. Infrared Millimeter Waves*, **29**(11), 1011 (2008).
11. M. Cengher, J. Lohr, I. A. Gorelov, W. H. Grosnickle, D. Ponce, P. Johnson, *Proc. 15th Joint Workshop Electron Cyclotron Emission and Electron Cyclotron Resonance Heating (EC-15)*, Yosemite, California, March 10-13, 2008, p. 483, J. Lohr, Ed., World Scientific Publishing Company, Singapore (2009).
12. R. A. Olstad, R. W. Callis, J. L. Doane, H. J. Grunloh, C. P. Moeller, *Proc. 15th Joint Workshop Electron Cyclotron Emission and Electron Cyclotron Resonance Heating (EC-15)*, Yosemite, California, March 10-13, 2008, p. 542, J. Lohr, Ed., World Scientific Publishing Company, Singapore (2009).
13. R. W. Callis, J. L. Doane, H. J. Grunloh, K. Kajiwara, A. Kasugai, C. P. Moeller, Y. Oda, R. A. Olstad, K. Sakamoto, K. Takahashi, *Fusion Eng. Des.*, **84**(2-6), 526 (2009).
14. S. Park, J. Jeong, W. Namkung, Moo-Hyun Cho, Y. S. Bae, Won-Soon Han, Hyung-Lyeol Yang, *Fusion Sci. Technol.*, **55**(1), 56 (2009).
15. M. A. Shapiro, E. J. Kowalski, J. R. Sirigiri, D. S. Tax, R. J. Temkin, T. S. Bigelow, J. B. Caughman, D. A. Rasmussen, *Fusion Sci. Technol.*, **57**(3), 196 (2010).
16. J. L. Doane, C. P. Moeller, *Int. J. Electronics*, **77**(4), 489 (1994).
17. J. Uher, J. Bornemann, U. Rosenberg, in Waveguide Components for Antenna Feed Systems: Theory and CAD (Artech House, Norwood, MA, 1993) pp. 9-51.
18. A. D. Olver, P. J. B. Clarricoats, A. A. Kishk, L. Shafai, Microwave Horns and Feeds, ed. by P. J. B. Clarricoats, Y. Rahmat-Samii, J. R. Wait (IEEE Press, New York, 1994), pp. 106-117.
19. J. M. Neilson, P. E. Latham, M. Caplan, W. G. Lawson, *IEEE Trans. Microw. Theory Tech.*, **37**(8), 1165 (1989).
20. G. G. Denisov, D. A. Lukovnikov, W. Kasparek, D. Wagner, *Int. J. Infrared Millimeter Waves*, **17**(5), 933 (1996).
21. E. J. Kowalski, D. S. Tax, M. A. Shapiro, J. R. Sirigiri, R. J. Temkin, T. S. Bigelow, D. A. Rasmussen, *IEEE Trans. Microw. Theory Tech.*, **58**(11), 2772 (2010).
22. Cascade User Manual, version 4.0. (Lexam Research, Redwood City, CA, 2013).
23. J. L. Doane, *Int. J. Infrared Millimeter Waves*, **14**(2), 363 (1993).
24. C. Dragone, *IEEE Trans. Microw. Theory Tech.*, **28**(7), 704 (1980).

25. E. A. Nanni, S. K. Jawla, M. A. Shapiro, P. P. Woskov, R. J. Temkin, *J. Infrared Millimeter Terahertz Waves* **33**(7), 695 (2012).